www.elsevier.com/locate/jbiomech

In vitro and in silico approaches to quantify the effects of the Mitraclip® system on mitral valve function

Francesco Sturla, Riccardo Vismara, Michal Jaworek, Emiliano Votta, Paolo Romitelli, Omar A. Pappalardo, Federico Lucherini, Carlo Antona, Gianfranco B. Fiore, Alberto Redaelli

PII: S0021-9290(16)31171-X
DOI: http://dx.doi.org/10.1016/j.jbiomech.2016.11.013
Reference: BM7974

To appear in: *Journal of Biomechanics*
Accepted date: 2 November 2016

Cite this article as: Francesco Sturla, Riccardo Vismara, Michal Jaworek Emiliano Votta, Paolo Romitelli, Omar A. Pappalardo, Federico Lucherini, Carl Antona, Gianfranco B. Fiore and Alberto Redaelli, In vitro and in silic approaches to quantify the effects of the Mitraclip® system on mitral valv function, *Journal of Biomechanics* http://dx.doi.org/10.1016/j.jbiomech.2016.11.013

In vitro and in silico approaches to quantify the effects of the Mitraclip® system on mitral valve function

Francesco Sturla[a], PhD, Riccardo Vismara[a], PhD, Michal Jaworek[a], MSc, Emiliano Votta[a], PhD, Paolo Romitelli[b], MSc, Omar A. Pappalardo[a,f], MSc, Federico Lucherini[a], MSc, Carlo Antona[c,d,e], MD, Gianfranco B. Fiore[a], PhD, Alberto Redaelli[a], PhD

[a] Department of Electronics, Information and Bioengineering, Politecnico di Milano, Milano, Italy

[b] Abbott Vascular International, Bruxelles, Belgium

[c] Forcardiolab, Fondazione per la ricerca in Cardiochirurgia ONLUS, Milan, Italy

[d] Cardiovascular Surgery Department, "Luigi Sacco" University general Hospital, Milan, Italy

[e] Università degli Studi di Milano, Milan, Italy

[f] Division of cardiovascular Surgery, Università degli Studi di Verona, Verona, Italy

Corresponding Author:

Francesco Sturla, PhD

Department of Electronics, Information and Bioengineering, Politecnico di Milano

Via Golgi 39, 20133 Milano

Italy

Phone: +39-02-2399-3327

email: francesco.sturla@polimi.it

Keywords: Mitral valve, Mitraclip®, Percutaneous procedure, Finite element models, Experimental platforms

Word Count: 3942

Special Issue of the Journal of Biomechanics on "*Biofluid Mechanics*"

ABSTRACT

Mitraclip® implantation is widely used as a valid alternative to conventional open-chest surgery in high-risk patients with severe mitral valve (MV) regurgitation. Although effective in reducing mitral regurgitation (MR) in the majority of cases, the clip implantation produces a double-orifice area that can results in altered MV biomechanics, particularly in term of hemodynamics and mechanical stress distribution on the leaflets.

In this scenario, we combined the consistency of in vitro experimental platforms with the versatility of numerical simulations to investigate clip impact on MV functioning. The fluid dynamic determinants of the procedure were experimentally investigated under different working conditions (from 40 bpm to 100 bpm of simulated heart rate) on six swine hearts; subsequently, fluid dynamic data served as realistic boundary conditions in a computational framework able to quantitatively assess the post-procedural MV biomechanics. The finite element model of a human mitral valve featuring an isolated posterior leaflet prolapse was reconstructed from cardiac magnetic resonance. A complete as well as a marginal, sub-optimal grasping of the leaflets were finally simulated.

The clipping procedure resulted in a properly coapting valve from the geometrical perspective in all the simulated configurations. Symmetrical complete grasping resulted in symmetrical distribution of the mechanical stress, while uncomplete asymmetrical grasping resulted in higher stress distribution, particularly on the prolapsing leaflet.

This work pinpointed that the mechanical stress distribution following the clipping procedure is dependent on the cardiac hemodynamics and has a correlation with the proper execution of the grasping procedure, requiring accurate evaluation prior to clip delivery.

Word Count: 250

1. INTRODUCTION

The mitral valve (MV) consists of two leaflets (anterior and posterior) anatomically splitted into three scallops (A1, A2, A3, and P1, P2, P3, respectively). Each leaflet inserts into the fibrous annulus at the valvular plane, and is connected to the left ventricle (LV) internal wall by means of chordae tendineae that originate from two papillary muscles. The physiological interplay between these sub-structures prevents the blood to flow from the LV to the left atrium (LA) during LV systole. Its alterations lead to mitral regurgitation (MR), the most common valvular pathology (Nkomo et al., 2006). The most frequent form of MR is the isolated prolapse of the posterior middle-scallop (P2) (Adams et al., 2010): due to the local degeneration of leaflet and chordae tissue, P2 invades the atrial volume without coapting with its counterpart, i.e. A2.

When MR is severe, life expectancy and quality are reduced (Denti et al., 2014), and symptomatic patients should be rapidly treated (Vahanian et al., 2013). Standard approach nowadays is conventional, open-chest surgery (Bonow et al., 2008) finalized to MV substitution or repair; however, as many as 49% of patients with severe MR are considered at high risk for conventional surgery (Mirabel et al., 2007), mainly due to age and associated comorbidities.

In this scenario, percutaneous approaches for the treatment of MR have emerged rapidly over the past few years as an alternative that can allow to treat inoperable or high risk patients (Denti et al., 2014; Feldman and Cilingiroglu, 2011). Among the currently available devices, the Mitraclip® (MC) system (Abbott Vascular, Inc., Menlo Park, California, US) is the most widely used transcatheter device (Feldman and Young, 2014). The device is intended to replicate, with a minimally invasive approach, a well-established surgical technique consisting in restoring MV coaptation by stitching the leaflets together creating a double-orifice valve (Alfieri et al., 2001). In the transcatheter approach (Fig. 1), the function of the stich is replaced by a clip delivered by a catheter in the LA under fluoroscopic or echographic guidance.

Several clinical trials (Feldman et al., 2009; Whitlow et al., 2012) compared the MC to the open-chest repair, and pointed out that the transcatheter approach is effective in reducing MR in the majority of cases, particularly in case of degenerative MR.

Nonetheless, MC implantation can induce biomechanical alterations in the valve functioning, which can be related to implant failure (Chanda and Venn, 2012; Puls et al., 2014). The standard P2-A2 grasping procedure results in a double-orifice diastolic configuration of the MV, which can induce increased diastolic transvalvular pressure drop (Biaggi et al., 2013; Wunderlich and Siegel, 2013). Moreover, the interaction between the clip and the grasped portion of the MV leaflet can induce altered local mechanical stress (Avanzini et al., 2011; Sturla et al., 2014).

In the present work, we focus on two aspects, which may have a potential impact on the hemodynamic and biomechanical outcomes of the MC procedure. The first one is related to the post-operative heart working conditions (e.g. rest, low or moderate exercise conditions), which depend on the actual heart rate (HR) and systemic pressure (P_s). The second aspect consists in the accuracy of the grasping maneuver. Indeed, the MV leaflet tissue can be grasped completely, i.e. the clip grasps the leaflet tissue for the entire length of its arm, or marginally; in the latter case, marginal grasping of the leaflet tissue of one (asymmetrical marginal grasping), or both the two MV leaflets (symmetrical marginal grasping) may occur. Accordingly, we investigated the impact of these aspects on the outcomes of the MC procedure combining in a systematic framework the consistency of *in vitro* experimental platform with the versatility of numerical simulations. A state-of-the-art pulsatile mock-loop system, designed to house entire swine hearts (Leopaldi et al., 2012; Vismara et al., 2016a; Vismara et al., 2016b), was used to assess post-procedural MV hemodynamics in MC-treated heart samples under different heart rate conditions, ranging between 40 and 100 bpm. Subsequently, *in vitro* pressure data served as realistic boundary conditions in a finite element (FE) model of the human MV derived from *in vivo* cardiac magnetic resonance (CMR) imaging and reporting an isolated P2 prolapse (Sturla et al., 2014). Here, we numerically assessed the impact of a P2-A2 clipping procedure on MV biomechanics, systematically combining the collected *in vitro* heart rate conditions with the different conditions of MV leaflets grasping, i.e. a complete grasping between A2 and P2 portions as well as a partial grasping of the leaflet tissue of one, or both the two MV leaflets.

2. MATERIALS AND METHODS

2.1 In-vitro analysis

We adopted a mock loop system (ML) designed to host entire explanted swine hearts activated as a passive structure by an external mechanical pump. This ML was exploited to replicate flow and pressure wave forms comparable with the typical *in vivo* curves and assess MV hemodynamics, while monitoring MV functioning through acquisition of high-quality echo and endoscopic images (Leopaldi et al., 2012).

Mock loop design – The ML system (Fig. 2a) consisted of: i. a programmable piston pump surgically connected to the LV via the apex, and capable of replicating systolic and diastolic flow rates; ii. a hydraulic afterload mimicking the systemic input impedance connected downstream from the AV; iii. an open-to-air preload connected to the left atrium. The pump forced the working fluid in the LV during the simulated systole. The fluid crossed the AV, enter the afterload, and from here, the hydraulic circuit closed into the preload. During the diastole, the pump retrieved fluid from the LV, and the preload yielded fluid to the LV through the MV. A detailed description of the experimental apparatus was published elsewhere (Leopaldi et al., 2012; Vismara et al., 2016a; Vismara et al., 2016b). The mock loop was equipped with three pressure transducers (PC140 series, Honeywell Inc., Morristown, NJ, USA) to measure pressure in the LA and in the LV (P_{LA} and P_{LV}, respectively), and in the impedance simulator (P_{sys}). A 1" probe of an ultrasound transit-time flowmeter (HT110r, Transonic Systems, Ithaca, USA) was connected downstream from the AV to acquire aortic flow rate.

Experimental protocol –The clip was implanted in six swine hearts with continent MV. These valves were intended to experimentally model a MV ideally and fully repaired with the clipping procedure. The hearts were harvested from the local slaughterhouse. Following the assessment of normal anatomy by expert cardiac surgeons, each sample was tested according to the following experimental procedure:

1. An expert operator implanted the clip between the A2 and P2 scallops of the MV (Fig. 2b).
2. Once clipped, the heart was connected to the experimental apparatus, and test ran in the following conditions:

a. Simulated physiologic conditions: HR was set at 60bpm. The afterload was set to simulate a diastolic/systolic systemic pressure (P_S) ranging 80/120mmHg;
b. Simulated low heart rate conditions. HR: 40bpm; P_S: 40/80mmHg;
c. Simulated mild exercise conditions. HR: 80bpm; P_S: 100/140mmHg;
d. Simulated moderate exercise conditions. HR: 100bpm; P_S: 120/180mmHg.

3. In each experimental point the following quantities were recorded and sampled at 200Hz:
   a. Atrial pressure (P_{LA});
   b. Ventricular pressure (P_{LV});
   c. Aortic flow rate (Q);
   d. Mean systemic pressure (P_S^{mean}).

For this experimental campaign, the working fluid was saline solution at room temperature. Throughout the analysis, imaging techniques were adopted to enhance the control of the MC implantation procedure, thus assuring repeatable conditions to record hemodynamic quantities. For this purpose, the procedure was monitored and guided by means of real-time 3D echocardiography (EPIQ 7G, Philips Medical System, Amsterdam, NL) using a transesophageal X7-2t probe (Fig. 2c) while a fiberscope (ENF-GP, Olympus Corp., Tokyo, Japan) inserted in the atrium was used as support imaging to evaluate MV leaflets grasping (Fig. 2d). Direct MV inspection confirmed complete apposition between MV leaflets during systole as well as the peculiar diastolic MV double-orifice configuration. The raw hydrodynamic data were analyzed to evaluate the following quantities: mean (ΔP_{dias}^{mean}) and maximum (ΔP_{dias}^{MAX}) diastolic pressure drop across the MV (from the difference between P_{LA} and P_{LV}) and mean (ΔP_{sys}^{mean}) and maximum (ΔP_{sys}^{MAX}) systolic pressure drop; from Q the cardiac output (CO) was calculated to assess that the working experimental working conditions were comparable to physiology; also the mean systemic pressure (P_S^{mean}) was monitored (Table 1). Statistical analysis was performed using GraphPad Prism 5 (GraphPad Software Inc., La Jolla, CA, USA): continuous variables were expressed as mean ± standard deviation and compared by analysis of variance for repeated measures; a *P*-value<0.05 was considered significant. *Post hoc* analysis was done by applying the Bonferroni test.

For each heart rate condition, the recorded time course of transmitral pressure drop (ΔP) was used as input, i.e. loading condition, of the numerical MV model.

2.2 Numerical analysis of Mitraclip® outcomes

MV numerical model - A male patient (57 years old), resembling the requirements for Mitraclip® procedure (Feldman et al., 2009), was submitted to a preoperative *cine* CMR acquisition (TX Achieva 3.0T, Philips Medical System, Eindhoven, Netherlands) before undergoing surgical repair of P2 prolapse due to primary chordal rupture; 30 breath-hold cardiac phases were acquired on 18 long-axis planes evenly rotated along the LV axis with isotropic in-plane resolution of 1.25 mm and a slice thickness of 8 mm (Sturla et al., 2015). Subsequently, the end-diastolic MV geometrical model was reconstructed in MATLAB (The MathWorks Inc., Natick, MA, United States), after manual tracing of MV substructures, by sampling Fourier functions approximating MV leaflets profile (Sturla et al., 2014). The MV model was then complemented by PM tips and marginal, basal and strut chordae tendinae (Stevanella et al., 2011). P2 prolapse was reproduced by removing marginal chordae according to intraoperative clinical evidence. MV leaflets were mapped through a triangulated mesh, prescribing a regionally varying thickness (Kunzelman et al., 2007), while chordae tendinae were modeled as truss elements. Annular and PMs kinematics was reproduced consistently to *cine* CMR data: although the LV anatomy was not modeled we exploited the tracing of both annular and PM points throughout the acquired CMR time-points to replicate their actual time-dependent 3D position. The nonlinear and anisotropic mechanical response of MV leaflets was included exploiting the strain energy function (SEF) proposed by (Lee et al., 2014) (Table S1). Also, the hyperelastic response of chordae tendinae was reproduced fitting uniaxial test data from fresh porcine MVs (Kunzelman and Cochran, 1990). All MV tissues were assumed homogeneous with a density equal to 10.4 g/cm^3 (Stevanella et al., 2011; Votta et al., 2007) to mimic blood inertial effects.

MV biomechanics after Mitraclip® implantation – The simulation of MC implantation was reproduced according to our recent FE approach (Sturla et al., 2014). The two arms of the device were modeled as two perfectly rigid rectangular plates (Abbott Laboratories, 2014); *ad hoc* boundary conditions were

automatically defined to drive the MC deployment (Fig. 3a) after initial positioning of the device between the A2 and P2 scallops, on the site of valvular defect (Fig. 3b). Subsequently, MV biomechanics was assessed throughout a cardiac cycle encompassing the different heart rate conditions (Fig. 3c): i) low heart rate (HR=40bpm), ii) physiological (HR=60bpm), iii) mild exercise (HR=80bpm) and iv) moderate exercise conditions (HR=100bpm), respectively. At this aim, the *in vitro* transmitral pressure drops (ΔP), recorded on the ML system at the different heart rates (Fig. 4e), were uniformly applied on the ventricular side of MV leaflets as time-dependent loading conditions for the CMR-derived MV model. Also, at each HR, four different conditions of MV leaflet grasping were analyzed (Fig. 3d): i) a complete grasping between A2 and P2 scallops, ii) a symmetrical marginal grasping between MV leaflets, an asymmetrical marginal grasping of the iii) posterior P2 scallop or the iv) anterior A2 scallop. All the simulations were run in the commercial solver ABAQUS/Explicit 6.10 (SIMULIA, Dassault Systèmes, Vélizy-Villacoublay). A general scale-penalty contact algorithm was adopted for MV leaflets (Stevanella et al., 2009) while contact slippage and separation were prevented between MV leaflets and the Mitraclip® arms. Further details are available in the supplementary material.

The impact of Mitraclip® implantation on MV biomechanics was assessed in terms of: i) MV coaptation depth (C_D) defined as the distance between leaflet coaptation and MV annular plane (Agricola et al., 2008) and the systolic excursion (S_E) of the MV leaflets body into the LA chamber (Lang et al., 2011); ii) MV double orifice area (DOA) computed at early diastole projecting the leaflets free margin on the annular least square plane; iii) the maximum principal stress (S_I) acting on MV leaflets, in particular on the A2 and P2 portion on the MV leaflets, close to Mitraclip® arms. In particular, S_I values were extracted on a pre-defined region of the leaflet (6 x 6mm) close to Mitraclip® arms and compared, at the different heart rates, by means of box (median, 25^{th} and 75^{th} percentiles) and whiskers (10^{th} and 90^{th} percentiles) plots.

3. RESULTS

3.1 In vitro hydrodynamic measurements

The Mitraclip® was successfully implanted and tested in the six hearts in all the foreseen fluid dynamic conditions, as monitored exploiting both echocardiographic and fluoroscopic facilities. Statistically different working conditions in terms of CO and pressures were recorded by varying the heart rate in the selected range. More in detail, the mean CO and the systemic pressure ranged respectively from 2.5±0.2 L/min and 58.2±5.6 mmHg at 40bpm, to 4.4+0.5 L/min and 125.8±7.5 mmHg at 100bpm (Table 1).

The mean (Fig. 4a) and maximum (Fig. 4b) systolic pressure drops across the clipped valve ranged respectively from 43.4±4.0 mmHg and 90.7±9.0 mmHg at 40 bpm, to 96.5±8.4 mmHg and 260.9±14.9 mmHg at 100 bpm. MV diastolic pressure drops mean (Fig. 4c) and maximum (Fig. 4d) values ranged respectively from 2.3±1.1 mmHg and 5.9±2.2 mmHg at 40 bpm, to 5.4±1.5 mmHg and 20.2±1.9 mmHg at 100 bpm.

The time course of the MV pressure drops (ΔP), recorded in the six hearts, is reported in Fig. 4e for each heart rate. These courses represented realistic loading conditions to replicate in the FEM model the peculiar conditions of low, mild and moderate exercise, respectively.

3.2 Impact of the implanted device on MV biomechanics

We numerically assessed the postoperative MV biomechanics focusing on the MV closed configuration at the systolic peak of transmitral pressure (peak systole) and the fully open MV configuration at the peak of diastolic pressure drop (peak diastole).

Systolic MV coaptation – MC procedure produced a complete MV coaptation independently from both the simulated heart rate and grasping condition (Fig. 5). However, passing from low heart rate (40bpm) to moderate exercise (100bpm) conditions, C_D progressively decreased from 8.0 mm to 5.0 mm while S_E increased above 4.0 mm. At 100bpm, the marginal symmetrical A2-P2 grasping configuration reported the highest C_D percentage reduction equal to -24% while a peak S_E value of 4.3 mm was computed on the prolapsing posterior leaflet when simulating a marginal P2 asymmetrical grasping.

Diastolic MV double orifice area – The simulated clip induced a double MV orifice with an almost symmetrical percentage DOA redistribution between the antero-lateral (45% ÷ 52%) and the postero-medial (48% ÷ 55%) orifices, respectively (Fig. 6). Though limited, a DOA variation up to 15% was noticed in case of posterior marginal grasping when comparing the different grasping conditions at the same HR, e.g. between the symmetrical (5.0 cm^2) and asymmetrical (4.4 cm^2) marginal grasping at 100bpm, as well as when comparing the single grasping condition at different HRs, e.g. at 40bpm (5.2 cm^2) vs 60bpm (4.5 cm^2) in the P2 marginal asymmetrical grasping.

MV mechanical stress – At peak systole (Fig. 7), a common pattern of S_I redistribution on MV leaflets was visible although, at HRs higher than 40 bpm, S_I magnitude progressively increased: in particular, on the anterior leaflet close to the insertion of structural chordae tendinae, peak S_I values of about 200 kPa were computed at 40 bpm while the mechanical peak S_I value was locally over 600 KPa at moderate HR (100 bpm). Close to the Mitraclip® arms, as highlighted in the box plots, S_I magnitude was higher on the posterior prolapsing leaflet (P2) and it markedly increased at mild and moderate HRs, respectively. Moreover, S_I varied according to the simulated grasping conditions: a complete grasping resulted in a comparable S_I redistribution between A2 and P2 scallops (Fig. 7a) while a marginal but symmetrical clipping reduced S_I on the non-prolapsing A2 scallop more than on the P2 prolapsing region (Fig. 7b). An asymmetrical marginal clipping relieved S_I on the marginally clipped portion of the posterior (Fig. 7c) or anterior (Fig. 7d) MV leaflet while the prolapsing P2 scallop, although well-anchored to the clip with respect to its anterior counterpart, exhibited the highest increase in S_I values (Fig. 7d).

At peak diastole (Fig. 8), a large extent of MV leaflets, distally from the MC implantation (e.g. close to antero-lateral and postero-medial MV commissures), was unloaded and exhibited S_I values below 50 kPa at any HR. On the contrary, high S_I stresses were concentrated on both A2 and P2 regions close to the clip, though S_I values remained below 200kPa, i.e. largely lower than the corresponding systolic S_I values. Also, both S_I magnitude and distribution proved to be dependent on the simulated grasping conditions. In the complete grasping configuration, S_I was comparable between A2 and P2 scallops: at higher HRs, S_I increased in magnitude and progressively extended towards the MV annulus on a larger portion of the

leaflets (Fig. 8a). A marginal but symmetrical clipping reduced S_I on the non-prolapsing A2 scallop more than on the P2 prolapsing scallop (Fig. 8b). At any HR, an asymmetrical marginal clipping (Fig. 8c-d) reported low S_I values on the non-prolapsing A2 scallop while a well-grasped but prolapsing P2 leaflet (Fig. 8d) exhibited twice as big S_I values on a considerable extent of the clipped scallop.

4. DISCUSSION

The investigating approach adopted in this work, based on a close interaction between experimental and computational platforms, allowed for a systematic study of the complex biomechanical scenario resulting from the Mitraclip® implant. In the experimental apparatus, even under moderate exercise conditions, the MC never induced clinically relevant alteration of the fluid dynamic determinants. The computational platform, adopting the experimental pressure drop curves as boundary conditions, allowed for a deep insight into specific potential issues of the procedure. The grasping simulated in the P2-prolapse MV model resulted in a complete MV coaptation. Remarkably, this occurred also when a sub-optimal implanting procedure was simulated, with the grasping involving only the marginal portion of one, or of both the leaflets. The mechanical stress close to the clip generally increased with HR, particularly during the systole, and resulted in a symmetrically distributed stress between P2 and A2 in case of symmetrical, complete grasping. The FE assessment of postoperative MV biomechanics underlined two aspects which can lead to a potential clinical suggestion.

Geometrical perspective - The first aspect consists in the postoperative MV anatomical configuration: all the simulations reported an adequate MV coaptation, with computed C_D values close to physiological values (Agricola et al., 2008), and a systolic excursion of the treated prolapsing leaflet lower than the value reported for patients with P2 prolapse (Clavel et al., 2015). The S_E and C_D trend was in accordance with the simulated working conditions. S_E increased and C_D decreased with simulated HRs: the systolic pressure drop across the MV increased with HR, pushing the closed valve toward the LA. Moreover, the simulated sub-optimal grasping conditions did not significantly affect both the closed and open MV configuration, as

demonstrated by S_E and C_D indexes and similar patterns (Fig. 8) and values (Fig. 6) of the double orifice area, respectively. Our results suggest that in the immediate post-operative scenario, the percutaneous procedure may be effective in maintaining MV competency although MV leaflets are not completely or asymmetrically grasped.

Biomechanical perspective - The second aspect relays in the distribution of the mechanical stress between the two leaflet, depending of the grasping procedure. In case of symmetrical and complete grasping (Fig. 7a and Fig 8a), both systolic and diastolic stresses were symmetrically distributed between the A2 and P2 scallops. This could suggest that the MC procedure, when performed at the best, could allow for a physiologic-like interplay between MV leaflets in bearing LV pressure. When both A2 and P2 segments were marginally grasped, the prolapsing P2 scallop experienced higher stresses (Fig. 7b and Fig. 8b) as compared to the A2. This may be associated to the minor number of P2 residual chordae to bear and redistribute the transmitral pressure load. The leaflet tension locally increases where the clip is constraining the P2 to the non-prolapsing A2 scallop. This asymmetric distribution of stress between the two scallop was even more evident when an asymmetric clipping was simulated, with a complete P2 grasping, and a marginal A2 grasping. This configuration resulted in a remarkable increase in mechanical stress on the P2 scallop, with the highest SI values recorded at any heart rate, both at systole (Fig. 7d) and diastole (Fig. 8d). Marginal grasping of the physiologic A2, which systolic geometrical configuration is defined by its chordae, may resemble a clip which is positioned deeper in the ventricle. This configuration in turn pulls the P2 prolapsing scallop deeper in the ventricle: while A2 mechanical stress is uniformly distributed by the correctly enrolled chordae tendinae, the P2 scallop is mainly sustained by the clip. This results suggests that the most detrimental grasping condition is those in which the prolapsing cusp is fully grasped, with its anatomical counterpart partially grasped.

Clinical implication - Both the two aspects here discussed confirm the importance of an accurate post-procedural evaluation of the grasping, prior to clip delivery. Indeed, the echo Doppler could indicate a good post-procedural outcome in terms of proper MV continence. However, good hemodynamic results could coexist with an incomplete and asymmetrical grasping, which in turn may be related to higher local

mechanical stress, with respect to those recorded with a symmetrical complete grasping procedure. Thus, echographic or fluoroscopic post-procedural evaluation of the implant is mandatory to confirm the proper positioning of the clip, independently from a good Doppler hemodynamic result.

5. CONCLUSION

We can take advantage of the synergy between the *in vitro* passive beating heart platform and the numerical MV modelling to deepen the complex scenario of Mitraclip® implantation. On the one hand, the *in vitro* analysis can allow for a real-time monitoring of the MC procedure, as in the actual catheterization laboratory (Cath Lab), and provide useful information regarding post-procedural MV hemodynamics. On the other hand, *in vitro* pressure data serve as boundary conditions to fully exploit in a realistic scenario the versatility of the FE mechanical stress analysis, which can pinpoint specific biomechanical implications and potentially support the clinical setting of the procedure.

6. LIMITATIONS

The present study has three main limitations.

First, the experimental campaign was specifically designed to allow for repeatable experimental conditions. In this perspective, a physiologic, continent MV as a model of ideally treated incontinent MV was adopted, in order to reduce intra-sample variability potentially related to a simulated degenerative MR (Gelpi et al., 2015). It should be considered, indeed, that the focus of the *ex-vivo* experimental activity was not the study of the clipping procedure per se, but was to provide repeatable and reliable fluid dynamic parameters to be used in the FE analysis.

Second, measured pressure drop peak values were slightly higher as compared to standard clinical literature. This was mainly due to inertances in the experimental setup and, although impacting on the magnitude of systolic mechanical stress, it does not diminish the comparative value of the analysis.

Third, our study was restricted to the FE analysis of the acute MV mechanical response following the MC procedure; more advanced and complex multiscale structural approaches (Bianchi et al., 2016; Zhang et al., 2016) will be required to elucidate possible phenomena of mid- and long-term mechano-driven soft tissue remodeling.

SUPPLEMENTARY MATERIAL

Supplementary data associated with this article can be found in the online version.

CONFLICT OF INTEREST

Paolo Romitelli is an employee of Abbott Vascular International, Brussel, Belgium.

AKNOWLEDGEMENTS

This work was supported by the European Commission within the Horizon 2020 Framework through the MSCA-ITN-ETN European Training Networks (project number 642458)

FIGURES

Figure 1. Schematic drawing of the Mitraclip® procedure: **a)** access of the Mitraclip® device into the left atrium (LA) through trans-septal puncture; **b)** Mitraclip® insertion into the left ventricle (LV); **c)** Mitraclip® positioning across the mitral orifice, in the region of MR, and closure of the arms. The clip can be repositioned until the results in term of MV regurgitation is deemed satisfactory; finally, **d)** it is released and the delivery system retracted. AV, aortic valve; MV, mitral valve; TV, tricuspid valve; RA, right atrium; MC, Mitraclip® device.

Figure 2. Experimental analysis. **a)** Photography of the ML system and its schematic including the left ventricle (LV), a pulse duplicator (PD), a systemic impedance simulator (SIS) and a pre-load reservoir (PR). **b)** clipping procedure performed in three swine explanted hearts between the highlighted A2 and P2 scallops of the MV. **c)** echocardiographic monitoring during in vitro MV testing: during diastole the typical MV double orifice is pointed out. **d)** Atrial view of the MV as acquired by means of a fiberscope control, during in vitro MV testing, at different heart rates (HR).

Figure 3. FE evaluation of the Mitraclip® procedure: **a)** FE set-up of Mitraclip® implantation (Sturla et al., 2014) from the initial open configuration of the device to the complete closure of the its arms. **b)** standard clipping procedure between the A2 and P2 scallops of the MV leaflets; **c)** numerical FE loading transmitral pressure conditions derived from *in vitro* measurements at 4 different heart rates (HR equal to 40, 60, 80 and 100 bpm, respectively); **d)** FE investigation of 4 different leaflet grasping conditions: complete, marginal symmetrical, marginal asymmetrical on the P2 scallop and marginal asymmetrical on the A2 scallop.

Figure 4. Hydrodynamic experimental results **(a-d)**, reported as mean ± standard deviation, evaluated over the tested heart samples at the different heart rates of 40, 60, 80 and 100 bpm, respectively. For each variable, a statistically significant difference ($P<0.05$) was found for all reported values. **e)** time course of the MV pressure drop (ΔP) recorded in the six hearts and used as input in the FE simulations.

Figure 5. Contour maps of the systolic excursion (S_E) of the MV leaflets into the LA chamber at the peak of systolic transmitral pressure, for each simulated condition of grasping at the different heart rates of 40, 60, 80 and 100 bpm, respectively; the maximum value (S_E^{MAX}) is reported for each simulation. Also, the values of MV coaptation depth (C_D) between A2 and P2 portions of MV leaflets are reported for each configuration.

Figure 6. Values of double orifice area (DOA) computed at the peak of diastolic transmitral pressure drop at the heart rate of 40, 60, 80 and 100 bpm, respectively. For each grasping condition, histograms point out the percentage subdivision of the computed DOA between the antero-lateral (AL) and postero-medial (PM) orifice, respectively.

Figure 7. Maximum principal stress (S_I) acting on MV leaflets at the peak of systolic transmitral pressure. S_I contour maps are reported for each tested MV configuration (central column). On the A2 (right column)

and P2 (left column) portion of the MV leaflets, S_I values were extracted from a pre-defined area proximal to Mitraclip® arms and compared: S_I values are reported at different heart rates (i.e. 40, 60, 80, 100 bpm) by means of box (median, 25^{th} and 75^{th} percentiles) and whiskers (10^{th} and 90^{th} percentiles) plots.

Figure 8. Maximum principal stress (S_I) acting on MV leaflets at peak of diastolic transmitral pressure. S_I contour maps are reported for each tested MV configuration (central column). On the A2 (right column) and P2 (left column) portion of the MV leaflets, S_I values were extracted from a pre-defined area proximal to Mitraclip® arms and compared: S_I values are reported at different heart rates (i.e. 40, 60, 80, 100 bpm), by means of box (median, 25^{th} and 75^{th} percentiles) and whiskers (10^{th} and 90^{th} percentiles) plots.

TABLES

Table 1

Hydrodynamic results, reported as mean ± standard deviation, evaluated over the tested heart samples at the different heart rates of 40, 60, 80 and 100 bpm, respectively.

	40 bpm	**60 bpm**	**80 bpm**	**100 bpm**	***p-value***
CO [l min^{-1}]	2.5 ± 0.2 [a,b,c]	3.2 ± 0.3 [d,e]	4.0 ± 0.2 [f]	4.4 ± 0.5	< 0.0001
$\mathbf{P_S}^{\mathbf{mean}}$ [mmHg]	58.2 ± 5.6 [a,b,c]	88.4 ± 5.4 [d,e]	106.7 ± 2.0 [f]	128.8 ± 7.5	<0.0001
$\mathbf{\Delta P_{dia}}^{\mathbf{mean}}$ [mmHg]	2.3 ± 1.1 [b,c]	2.6 ± 0.7 [e]	3.8 ± 1.4 [f]	5.4 ± 1.5	< 0.0001
$\mathbf{\Delta P_{sys}}^{\mathbf{mean}}$ [mmHg]	43.4 ± 3.99 [a,b,c]	66.8 ± 3.4 [d,e]	80.4 ± 7.1 [f]	96.5 ± 8.4	< 0.0001
$\mathbf{\Delta P_{sys}}^{\mathbf{MAX}}$ [mmHg]	90.7 ± 9.0 [a,b,c]	156.7 ± 12.7 [d,e]	197.3 ± 12.7 [f]	260.9 ± 14.9	< 0.0001
$\mathbf{\Delta P_{dia}}^{\mathbf{MAX}}$ [mmHg]	5.9 ± 2.2 [b,c]	8.6 ± 2.5 [e]	12.3 ± 3.6 [f]	20.2 ± 1.9	< 0.0001

[a] 40 vs 60 $p < 0.05$
[b] 40 vs 80 $p < 0.05$
[c] 40 vs 100 $p < 0.05$
[d] 60 vs 80 $p < 0.05$
[e] 60 vs 100 $p < 0.05$
[f] 80 vs 100 $p < 0.05$

CO = cardiac output; $\mathbf{P_S}^{\mathbf{mean}}$= mean systemic pressure $\mathbf{\Delta P_{dia}}^{\mathbf{mean}}$= mean diastolic transmitral pressure; $\mathbf{\Delta P_{sys}}^{\mathbf{mean}}$= mean systolic transmitral pressure; $\mathbf{\Delta P_{sys}}^{\mathbf{MAX}}$= maximum systolic transmitral pressure; $\mathbf{\Delta P_{dias}}^{\mathbf{MAX}}$= maximum diastolic transmitral pressure.

REFERENCES

Abbott Laboratories, 2014. Electronic instructions for use for the Mitraclip(R) clip delivery system(http://www.abbottvascular.com/static/cms_workspace/pdf/ifu/structural_heart/eIFU_Mitraclip.pdf).

Adams, D.H., Rosenhek, R., Falk, V., 2010. Degenerative mitral valve regurgitation: best practice revolution. Eur Heart J 31, 1958-1966.

Agricola, E., Oppizzi, M., Pisani, M., Meris, A., Maisano, F., Margonato, A., 2008. Ischemic mitral regurgitation: mechanisms and echocardiographic classification. Eur J Echocardiogr 9, 207-221.

Alfieri, O., Maisano, F., De Bonis, M., Stefano, P.L., Torracca, L., Oppizzi, M., La Canna, G., 2001. The double-orifice technique in mitral valve repair: a simple solution for complex problems. J Thorac Cardiovasc Surg 122, 674-681.

Avanzini, A., Donzella, G., Libretti, L., 2011. Functional and structural effects of percutaneous edge-to-edge double-orifice repair under cardiac cycle in comparison with suture repair. Proc Inst Mech Eng H 225, 959-971.

Biaggi, P., Felix, C., Gruner, C., Herzog, B.A., Hohlfeld, S., Gaemperli, O., Stahli, B.E., Paul, M., Held, L., Tanner, F.C., Grunenfelder, J., Corti, R., Bettex, D., 2013. Assessment of mitral valve area during percutaneous mitral valve repair using the Mitraclip system: comparison of different echocardiographic methods. Circ Cardiovasc Imaging 6, 1032-1040.

Bianchi, D., Marino, M., Vairo, G., 2016. An integrated computational approach for aortic mechanics including geometric, histological and chemico-physical data. J Biomech 49, 2331-2340.

Bonow, R.O., Carabello, B.A., Chatterjee, K., de Leon, A.C., Jr., Faxon, D.P., Freed, M.D., Gaasch, W.H., Lytle, B.W., Nishimura, R.A., O'Gara, P.T., O'Rourke, R.A., Otto, C.M., Shah, P.M., Shanewise, J.S., 2008. 2008 Focused update incorporated into the ACC/AHA 2006 guidelines for the management of patients with valvular heart disease: a report of the American College of Cardiology/American Heart Association Task Force on Practice Guidelines (Writing Committee to Revise the 1998 Guidelines for the Management of Patients With Valvular Heart Disease): endorsed by the Society of Cardiovascular Anesthesiologists, Society for Cardiovascular Angiography and Interventions, and Society of Thoracic Surgeons. Circulation 118, 26.

Chanda, B., Venn, G.E., 2012. Mitral valve replacement following a failed Mitraclip procedure. Eur J Cardiothorac Surg 42, 739-740.

Clavel, M.A., Mantovani, F., Malouf, J., Michelena, H.I., Vatury, O., Jain, M.S., Mankad, S.V., Suri, R.M., Enriquez-Sarano, M., 2015. Dynamic phenotypes of degenerative myxomatous mitral valve disease: quantitative 3-dimensional echocardiographic study. Circ Cardiovasc Imaging 8.

Denti, P., Maisano, F., Alfieri, O., 2014. Devices for mitral valve repair. J Cardiovasc Transl Res 7, 266-281.

Feldman, T., Cilingiroglu, M., 2011. Percutaneous leaflet repair and annuloplasty for mitral regurgitation. J Am Coll Cardiol 57, 529-537.

Feldman, T., Kar, S., Rinaldi, M., Fail, P., Hermiller, J., Smalling, R., Whitlow, P.L., Gray, W., Low, R., Herrmann, H.C., Lim, S., Foster, E., Glower, D., 2009. Percutaneous mitral repair with the Mitraclip system: safety and midterm durability in the initial EVEREST (Endovascular Valve Edge-to-Edge REpair Study) cohort. J Am Coll Cardiol 54, 686-694.

Feldman, T., Young, A., 2014. Percutaneous approaches to valve repair for mitral regurgitation. J Am Coll Cardiol 63, 2057-2068.

Gelpi, G., Romagnoni, C., Vismara, R., Mangini, A., Contino, M., Fiore, G.B., Antona, C., 2015. Intracardiac Visualization of Transcatheter Mitral Valve Repair in an In Vitro Passive Beating Heart. Circulation 132, e131-132.

Kunzelman, K.S., Cochran, R.P., 1990. Mechanical properties of basal and marginal mitral valve chordae tendineae. ASAIO Trans 36, M405-408.

Kunzelman, K.S., Einstein, D.R., Cochran, R.P., 2007. Fluid-structure interaction models of the mitral valve: function in normal and pathological states. Philos Trans R Soc Lond B Biol Sci 362, 1393-1406.

Lang, R.M., Tsang, W., Weinert, L., Mor-Avi, V., Chandra, S., 2011. Valvular heart disease. The value of 3-dimensional echocardiography. J Am Coll Cardiol 58, 1933-1944.

Lee, C.H., Amini, R., Gorman, R.C., Gorman, J.H., 3rd, Sacks, M.S., 2014. An inverse modeling approach for stress estimation in mitral valve anterior leaflet valvuloplasty for in-vivo valvular biomaterial assessment. J Biomech 47, 2055-2063.

Leopaldi, A.M., Vismara, R., Lemma, M., Valerio, L., Cervo, M., Mangini, A., Contino, M., Redaelli, A., Antona, C., Fiore, G.B., 2012. In vitro hemodynamics and valve imaging in passive beating hearts. J Biomech 45, 1133-1139.

May-Newman, K., Yin, F.C., 1998. A constitutive law for mitral valve tissue. J Biomech Eng 120, 38-47.

Mirabel, M., Iung, B., Baron, G., Messika-Zeitoun, D., Detaint, D., Vanoverschelde, J.L., Butchart, E.G., Ravaud, P., Vahanian, A., 2007. What are the characteristics of patients with severe, symptomatic, mitral regurgitation who are denied surgery? Eur Heart J 28, 1358-1365.

Nkomo, V.T., Gardin, J.M., Skelton, T.N., Gottdiener, J.S., Scott, C.G., Enriquez-Sarano, M., 2006. Burden of valvular heart diseases: a population-based study. Lancet 368, 1005-1011.

Puls, M., Tichelbacker, T., Bleckmann, A., Hunlich, M., von der Ehe, K., Beuthner, B.E., Ruter, K., Beissbarth, T., Seipelt, R., Schondube, F., Hasenfuss, G., Schillinger, W., 2014. Failure of acute procedural success predicts adverse outcome after percutaneous edge-to-edge mitral valve repair with Mitraclip. EuroIntervention 9, 1407-1417.

Stevanella, M., Maffessanti, F., Conti, C., Votta, E., Arnoldi, A., Lombardi, M., Parodi, O., Caiani, E., Redaelli, A., 2011. Mitral Valve Patient-Specific Finite Element Modeling from Cardiac MRI: Application to an Annuloplasty Procedure. Cardiovasc Eng Tech 2, 66-76.

Stevanella, M., Votta, E., Redaelli, A., 2009. Mitral valve finite element modeling: implications of tissues' nonlinear response and annular motion. J Biomech Eng 131, 4000107.

Sturla, F., Onorati, F., Votta, E., Stevanella, M., Milano, A., Pechlivanidis, K., Puppini, G., Redaelli, A., Faggian, G., 2015. Repair of Mitral Valve Prolapse Through ePTFE Neochordae: A Finite Element Approach From CMR, in: Lenarz, T., Wriggers, P. (Eds.), Biomedical Technology. Springer International Publishing, pp. 117-128.

Sturla, F., Redaelli, A., Puppini, G., Onorati, F., Faggian, G., Votta, E., 2014. Functional and Biomechanical Effects of the Edge-to-Edge Repair in the Setting of Mitral Regurgitation: Consolidated Knowledge and Novel Tools to Gain Insight into Its Percutaneous Implementation. Cardiovasc Eng Tech, 1-24.

Vahanian, A., Alfieri, O., Andreotti, F., Antunes, M.J., Baron-Esquivias, G., Baumgartner, H., Borger, M.A., Carrel, T.P., De Bonis, M., Evangelista, A., Falk, V., Iung, B., Lancellotti, P., Pierard, L., Price, S., Schafers, H.J., Schuler, G., Stepinska, J., Swedberg, K., Takkenberg, J., Von Oppell, U.O., Windecker, S., Zamorano, J.L., Zembala, M., 2013. [Guidelines on the management of valvular heart disease (version 2012). The Joint Task Force on the Management of Valvular Heart Disease of the European Society of Cardiology (ESC) and the European Association for Cardio-Thoracic Surgery (EACTS)]. G Ital Cardiol 14, 167-214.

Vismara, R., Gelpi, G., Prabhu, S., Romitelli, P., Troxler, L.G., Mangini, A., Romagnoni, C., Contino, M., Van Hoven, D.T., Lucherini, F., Jaworek, M., Redaelli, A., Fiore, G.B., Antona, C., 2016a. Transcatheter Edge-to-Edge Treatment of Functional Tricuspid Regurgitation in an Ex Vivo Pulsatile Heart Model. J Am Coll Cardiol 68, 1024-1033.

Vismara, R., Leopaldi, A.M., Piola, M., Asselta, C., Lemma, M., Antona, C., Redaelli, A., van de Vosse, F., Rutten, M., Fiore, G.B., 2016b. In vitro assessment of mitral valve function in cyclically pressurized porcine hearts. Med Eng Phys 38, 346-353.

Votta, E., Maisano, F., Bolling, S.F., Alfieri, O., Montevecchi, F.M., Redaelli, A., 2007. The Geoform disease-specific annuloplasty system: a finite element study. Ann Thorac Surg 84, 92-101.

Whitlow, P.L., Feldman, T., Pedersen, W.R., Lim, D.S., Kipperman, R., Smalling, R., Bajwa, T., Herrmann, H.C., Lasala, J., Maddux, J.T., Tuzcu, M., Kapadia, S., Trento, A., Siegel, R.J., Foster, E., Glower, D., Mauri, L., Kar, S., 2012. Acute and 12-month results with catheter-based mitral valve leaflet repair: the EVEREST II (Endovascular Valve Edge-to-Edge Repair) High Risk Study. J Am Coll Cardiol 59, 130-139.

Wunderlich, N.C., Siegel, R.J., 2013. Peri-interventional echo assessment for the Mitraclip procedure. European Heart Journal - Cardiovascular Imaging 14, 935-949.

Zhang, W., Ayoub, S., Liao, J., Sacks, M.S., 2016. A meso-scale layer-specific structural constitutive model of the mitral heart valve leaflets. Acta biomaterialia 32, 238-255.

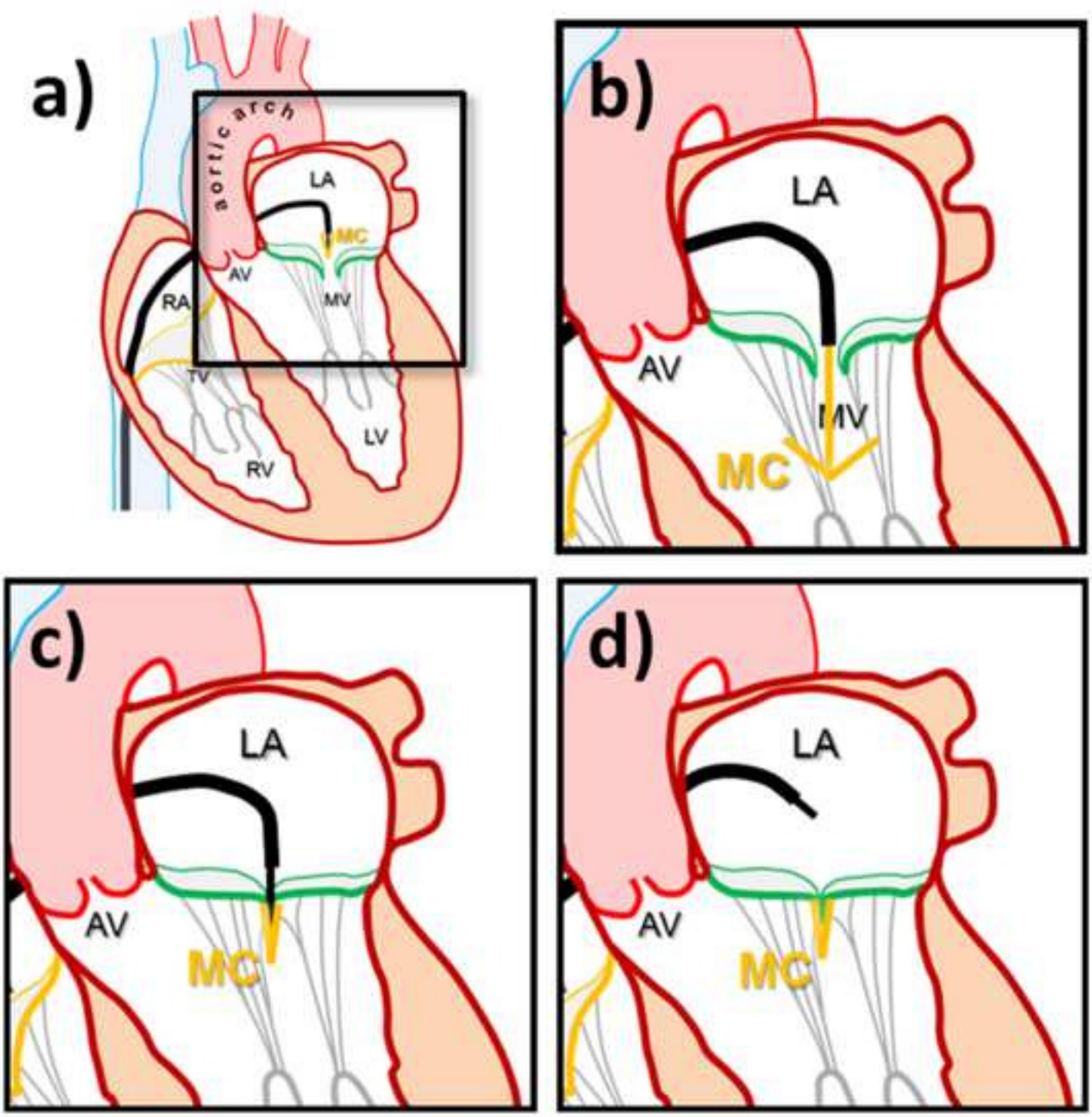

a) Mock loop system (IPML)

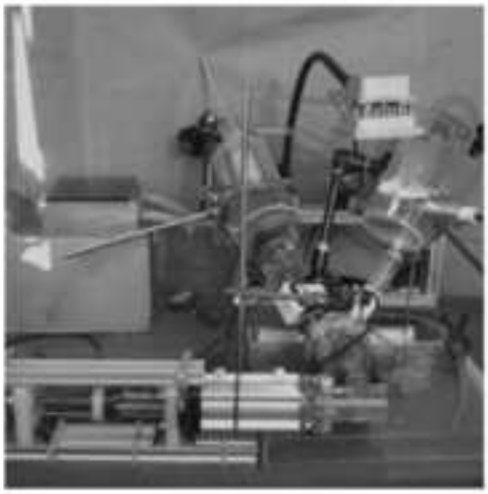

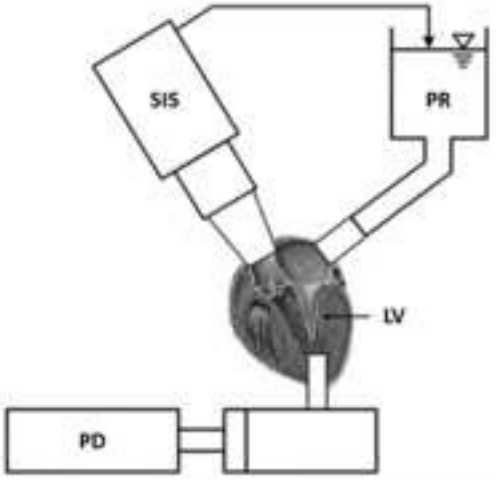

b) *In vitro* Mitraclip procedure

c) Echocardiography monitoring

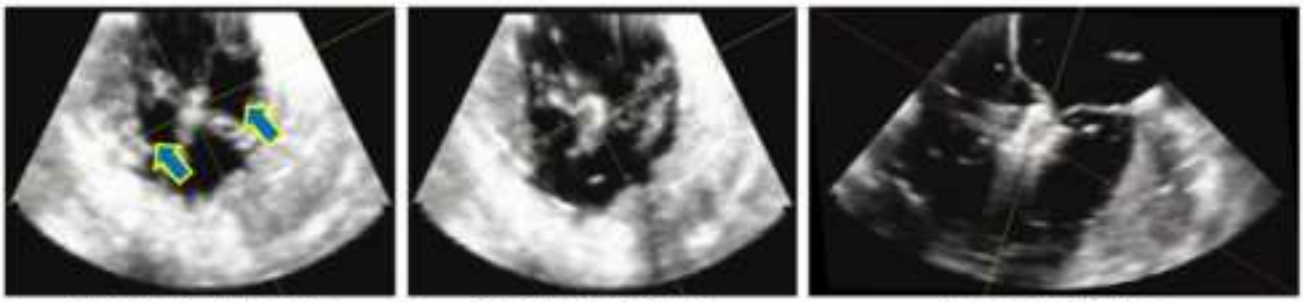

Short axis - Diastole | Short axis - Systole | Long axis - Systole

d) Fiberscope control

Systole	Diastole	Diastole	Diastole	Diastole
HR = 60bpm	HR = 40 bpm	HR = 60 bpm	HR = 80 bpm	HR = 100 bpm

Figure_3

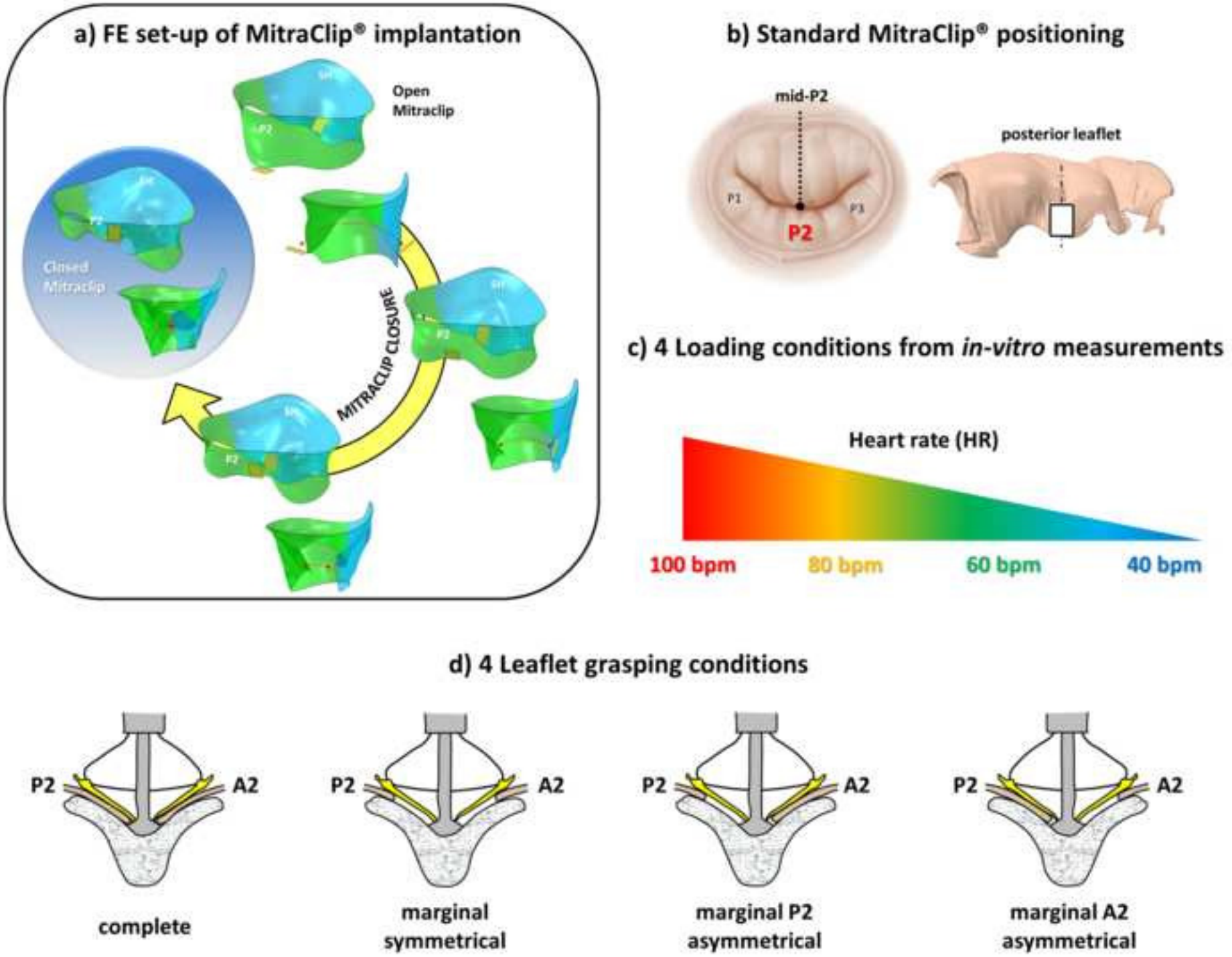

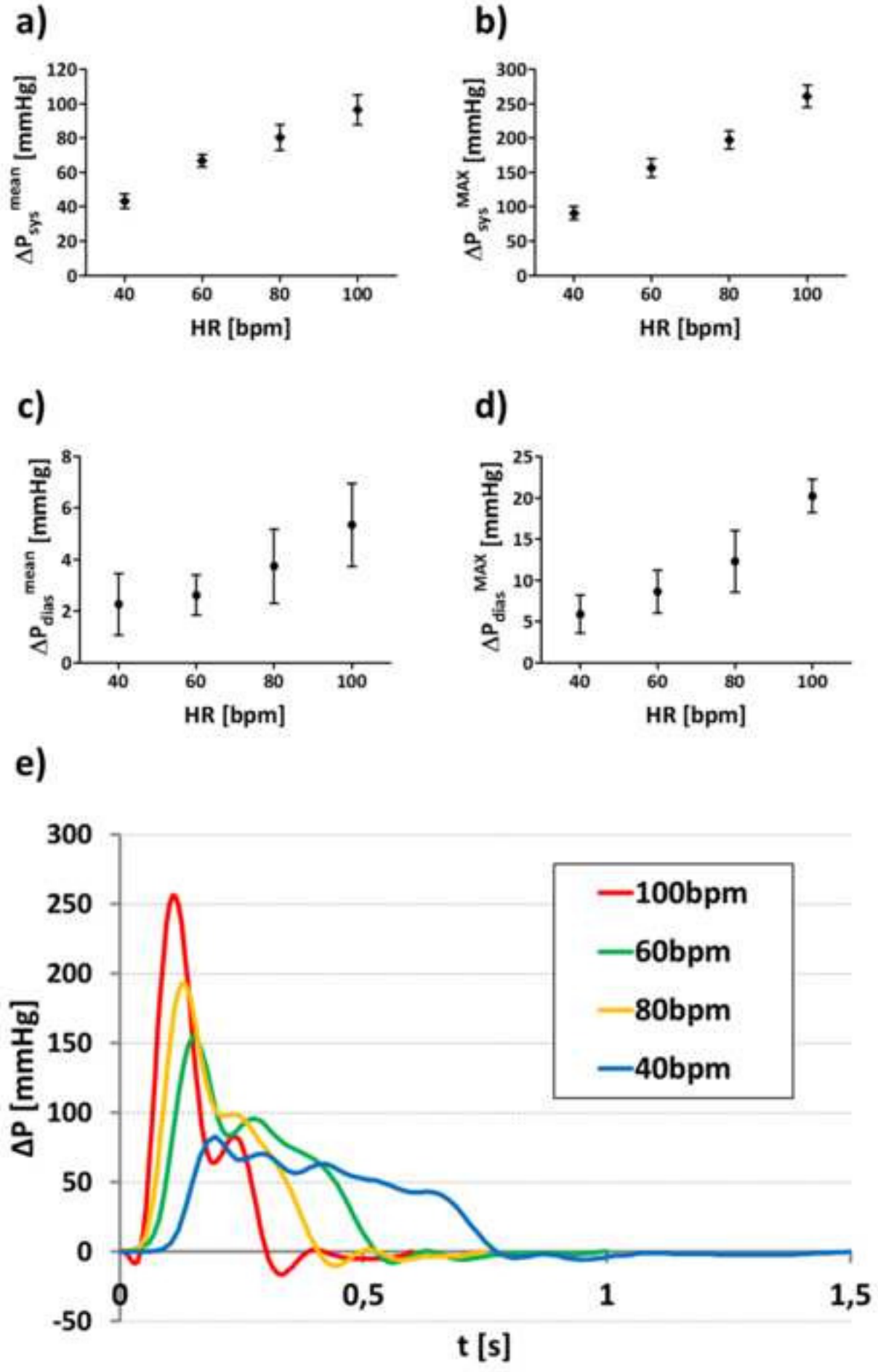

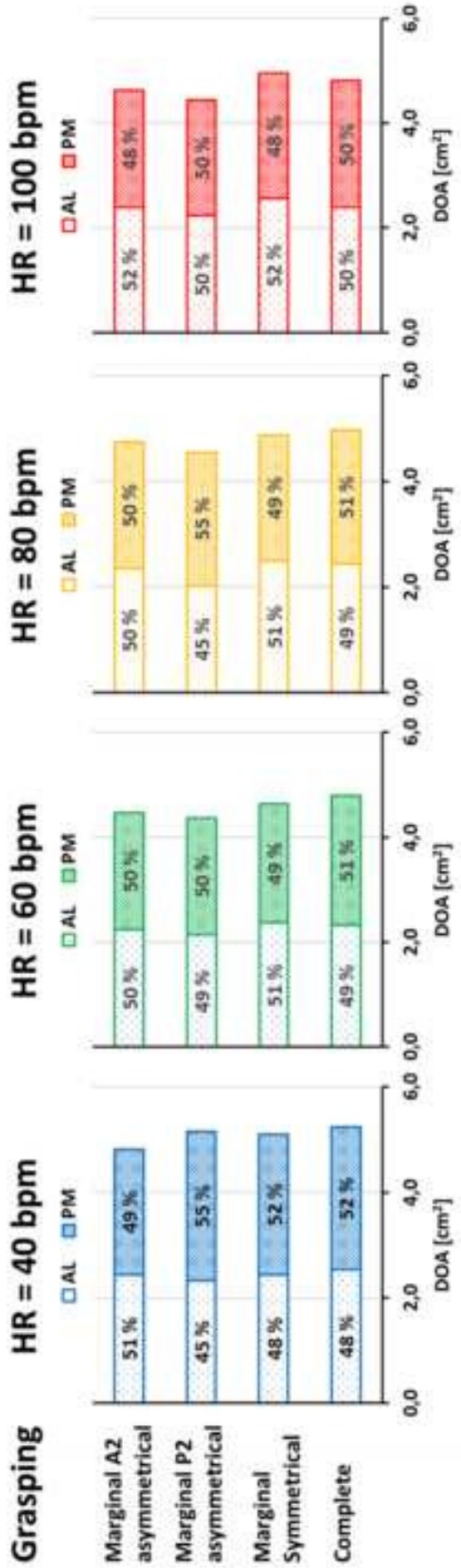
Grasping
HR = 40 bpm
HR = 60 bpm
HR = 80 bpm
HR = 100 bpm
AL
PM
DOA [cm²]
0,0
2,0
4,0
6,0
Marginal A2 asymmetrical
Marginal P2 asymmetrical
Marginal Symmetrical
Complete
51 %
49 %
45 %
55 %
48 %
52 %
48 %
52 %
50 %
50 %
49 %
50 %
51 %
49 %
49 %
51 %
50 %
50 %
45 %
55 %
51 %
49 %
49 %
51 %
52 %
48 %
50 %
50 %
52 %
48 %
50 %
50 %

Figure_5

Figure_6

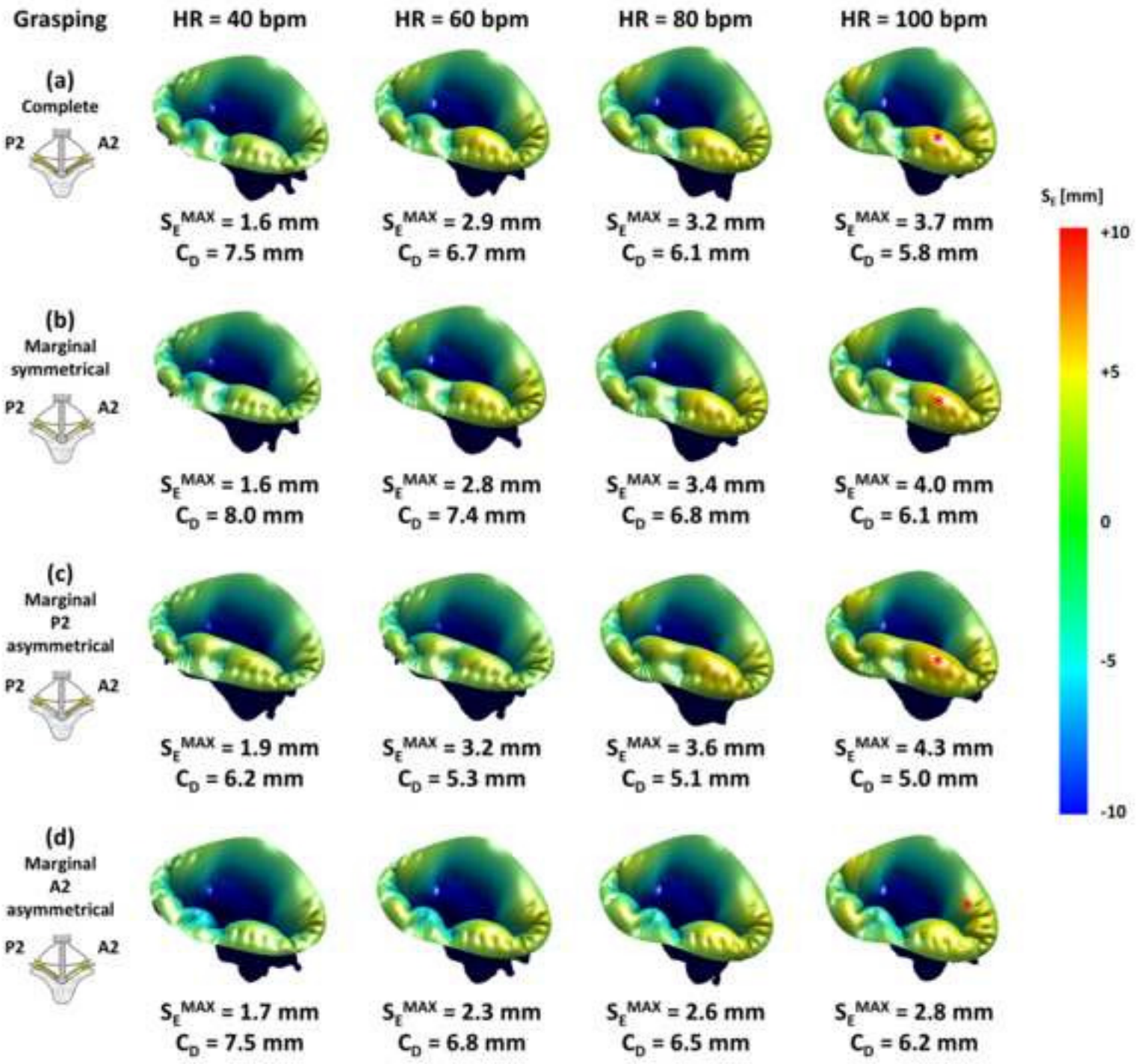

Figure_7

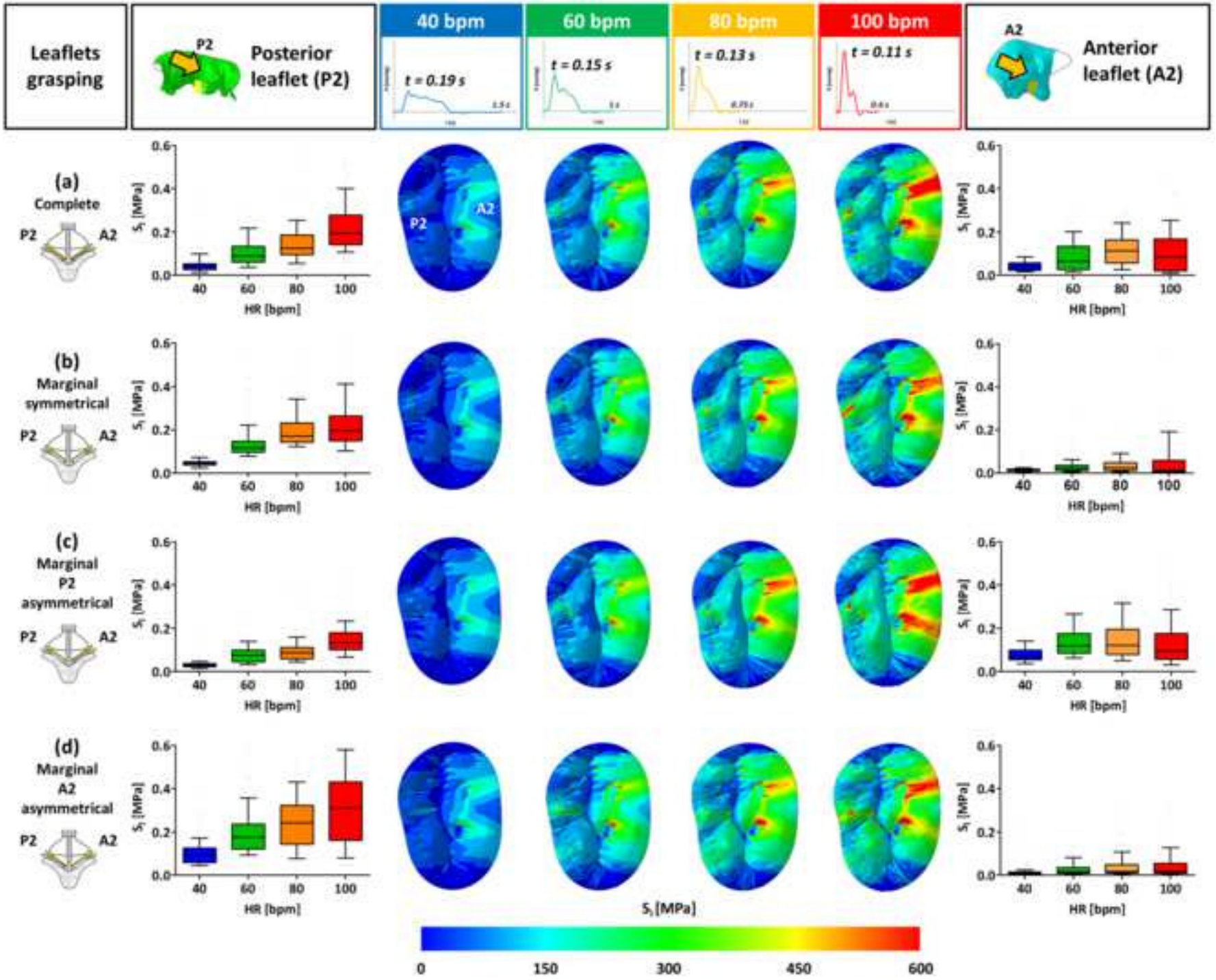

Figure_8